DOI: 10.1002/chem.200700927

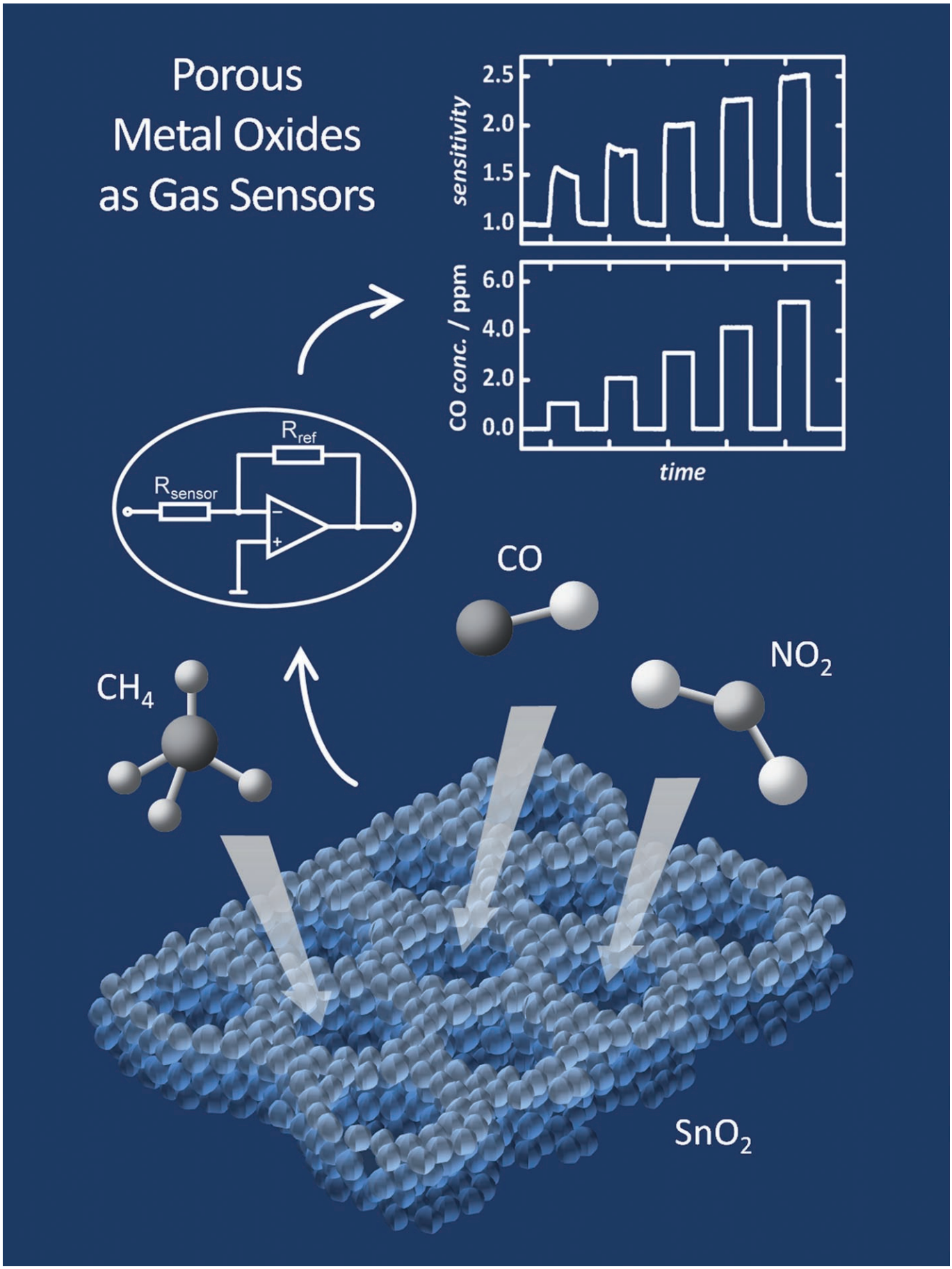

Porous Metal Oxides as Gas Sensors

Michael Tiemann*[a]

Abstract: Semiconducting metal oxides are frequently used as gas-sensing materials. Apart from large surface-to-volume ratios, well-defined and uniform pore structures are particularly desired for improved sensing performance. This article addresses the role of some key structural aspects in porous gas sensors, such as grain size and agglomeration, pore size or crack-free film morphology. New synthesis concepts, for example, the utilisation of rigid matrices for structure replication, allow to control these parameters independently, providing the opportunity to create self-diagnostic sensors with enhanced sensitivity and reproducible selectivity.

Keywords: mesoporous materials · nanostructures · semiconductors · sensors · thin films

Introduction

Almost half a century ago it was realised that semiconducting metal oxides have great potential as gas-sensing materials, owing to the fact that chemical interaction of gas molecules with the semiconductor's surface leads to changes in the electrical conductivity (Figure 1).[1] Such "chemiresistors" can be manufactured as portable devices that are operated at elevated temperature by battery power supply and used in a large variety of applications, including the detection of hazardous gases in factory plants or mining facilities, oxygen control in combustion exhaust car emission or humidity and air quality control (hydrocarbons, nitric oxides) in automobile cabins or living spaces.[2,3] The sensing material is usually deposited as a polycrystalline film or layer on a

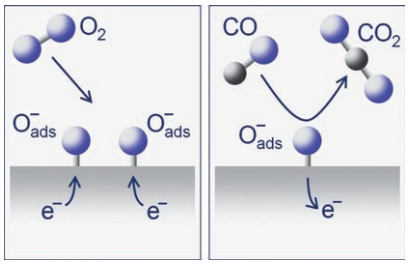

Figure 1. Simplified schematic representation of chemical reactions occurring at the surface of a semiconducting (n-type) gas sensor according to a standard model. Left: Chemisorption of oxygen from the gas phase (air) leads to the immobilisation of conduction electrons in the near-surface region. Right: reducing gases (e.g., CO) abstract surface-bound oxygen, thereby releasing electrons back into the crystal. Thus, the electric conductivity is a measurable for the concentration of the reducing gas. (The true nature of the adsorbed oxygen species is subject to discussion.[12])

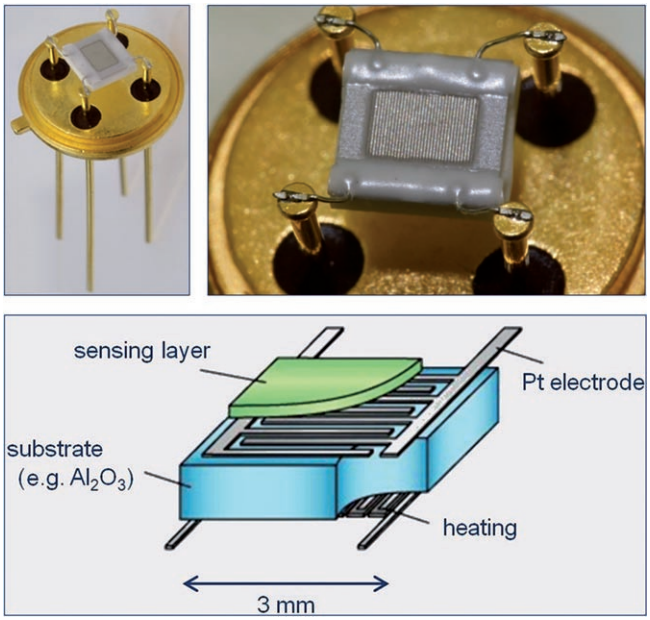

Figure 2. Photographs (top) and schematic drawing (bottom) of an example sensor substrate (UST Umweltsensortechnik GmbH, Germany). The sensor material is deposited on the interdigitated Pt electrode structure, for example, by drop-coating.)

[a] Dr. M. Tiemann
Institut für Anorganische und Analytische Chemie
Justus-Liebig-Universität, Heinrich-Buff-Ring 58
35392 Giessen (Germany)
Fax: (+49) 641-9934-109
E-mail: michael.tiemann@anorg.chemie.uni-giessen.de

substrate with integrated electrodes and heating (Figure 2). Extensive scientific and engineering research is being dedicated to the optimization of semiconducting gas sensors with respect to their sensitivity, response rate, gas selectivity and economic efficiency (low manufacturing costs, low operating temperatures). From the large number of scientific publications that have been summarised in several recent review articles,[2–11] it is apparent that the physics and chemistry of semiconducting gas sensors is complex and still not exhaustively understood. Several factors contributing to the working principles have been identified, but it is often difficult to separate them from each other in order to study their individual impact on the overall sensor performance.

In semiconducting metal oxides oxygen vacancies that act as electron donors (n-type semiconductors) or excess oxygen atoms that act as electron acceptors (p-type) are responsible for the electronic conductance. SnO_2 (n-type) is the most frequently used semiconducting material for gas sensing. The mechanisms responsible for gas sensing are not fully understood and subject to ongoing discussion.[12] According to a standard model, chemisorption of oxygen from the gas phase creates extrinsic surface acceptor states that immobilize conduction band electrons from the near-surface region of an n-type semiconductor,[13] as depicted in a simplified fashion in Figure 1 (left). Under ambient conditions, that is, in the presence of air, the near-surface region of each grain is therefore depleted of electrons (depletion layer), relative to the interior parts; the surface coverage with oxygen functionalities is at equilibrium. In the depletion layer the conductance is lower as compared to the absence of oxygen gas. As long as neighbouring grains are in contact with each other the same applies to the overall conductance of the entire material. For p-type semiconductors the chemisorption of oxygen leads to an accumulation surface layer and, thus, to a higher conductance. The presence of other gases with either reducing or oxidising properties will further affect the density of charge carriers (n-type electrons or p-type holes) in the near-surface region of each grain. Reducing gas molecules (e.g. CO) will abstract surface-bound oxygen atoms, a process that releases immobilised electrons, as schematically depicted in Figure 1 (right). In contrast, oxidising gases (e.g. NO_2) immobilise further conduction-band electrons from the near-surface region by creating additional surface-acceptor states. As a result, the foreign gas molecules cause a decrease (reducing gases) or increase (oxidising gases) of the depletion layer thickness by changing the surface-state density, which in turn leads to a change in the net conductance of the material. Thus, the conductance is a measurable quantity as a sensor signal for the concentration of such gases. It should be noted, though, that the above-made considerations describe the physicochemical principles of gas sensing in a highly idealised way. Several additional factors that make the situation a lot more complicated are neglected; for example, the aspect of humidity or partial deactivation of the sensor's surface by irreversible adsorption of gas molecules are not discussed here. A more comprehensive description of the underlying principles in semiconducting gas sensors can be found, for instance, in the above-mentioned review articles.[2–11]

The most important properties of a gas sensor are its sensitivity, operating temperature, selectivity and long-term stability. In other words, a good gas sensor should 1) show a strong and noise-free change in conductance upon changes in the target gas concentration, 2) show no or little response to gases other than the target gas (especially water), 3) still deliver reliable performance after prolonged usage and 4) be applicable at low temperature to minimise energy consumption (unless for reasons of surface chemistry high temperatures are necessary).

In the following we will discuss how control over structural and textural properties of the sensing materials may be used to improve the sensors' properties with respect to the above-mentioned requirements. In particular, the role of porosity will be discussed. Based on their properties with respect to physisorption phenomena, porous materials are classified according to their pore sizes.[14] If the pore width is between 2 and 50 nm the material is called "mesoporous"; this is the relevant pore size regime for porous semiconductor gas sensors that we will focus on in the following. Materials with smaller or larger pores are called "microporous" or "macroporous", respectively.

Conventional Synthesis Methods for Porous Semiconducting Metal Oxides

Conventional sol–gel synthesis procedures[15] aim to create solid networks built up from particles with sizes in the region of a few nanometers. The particles are formed under mild synthesis conditions in liquid (usually aqueous) medium by condensation of dissolved precursor species. As a result, a monodisperse colloidal dispersion (the sol) is obtained. The dispersed particles may be either amorphous or crystalline; their shape is usually approximately spherical and their size can be adjusted by choice of the respective synthesis parameters, for example, precursor concentration or synthesis temperature. Subsequent cross-linking of the sol particles then leads to gelation, that is, a continuous porous network (the gel) is formed in the liquid environment. Finally, the solvent is removed from the gel to yield the porous solid, which may be subjected to calcination in order to improve its stability. Both the solvent removal (e.g., by evaporation) and the calcination procedure often lead to significant densification of the material, that is, a substantial part of the porosity is lost, unless special solvent removal procedures, such as supercritical drying, are applied. To obtain a porous film on a substrate the sol may be directly applied to the substrate before gelation, for example, by spin-coating or dip-coating.

In a quite representative synthesis protocol, Yamazoe et al. have synthesised SnO_2 for gas sensing by preparing sols form $SnCl_4$ at pH 10.5.[16] Depending on the precursor concentration, stable particles with diameters between 7 and 13 nm were obtained by hydrothermal treatment at 200 °C

for 3 h, as determined by TEM and powder X-ray diffraction (using the Scherrer method). Thin films (< 1 μm) were obtained by spin-coating and subsequent calcination at 600 °C (Figure 3). The interparticle voids (pore sizes) were

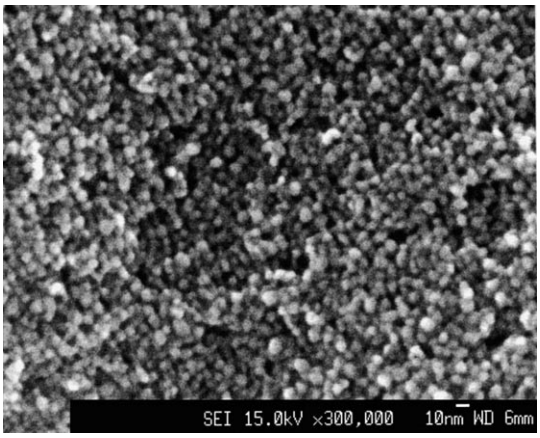

Figure 3. Scanning electron microscope (SEM) image of a SnO_2 film (thickness < 1 μm, top view) prepared from a sol by spin coating and subsequent calcination at 600 °C; the grains are about 10 nm in size.[16b]

assumed to be uniform and in the range of small mesopores, although no porosity measurements were provided. Further syntheses by the same group succeeded in more elaborate control over particle sizes by adjusting the pH (10–12) and the hydrothermal treatment conditions (200–250 °C).[17] Lu et al. have applied supercritical drying to the sol–gel synthesis of SnO_2 thick films with mean particle sizes around 4–8 nm to obtain large mesopores between 13 and 15 nm; the materials were used for simultaneous sensing of CO, CH_4 and H_2.[18,19] Organically modified tin precursors were used by Jitianu and Wark et al. to synthesise 15–25 nm sized SnO_2 particles for optical gas sensing.[20] Egashira et al. prepared mesoporous TiO_2 from $Ti(NO_3)_4$ by the sol–gel technique, utilising polyethylene glycol (PEG) as a porogen; the as-synthesised products exhibited large specific surface areas, but lost some porosity after calcination at 600 °C.[21] Further sol–gel syntheses of porous semiconducting metal oxides for gas sensing are listed in reference [8]. Sol–gel-derived syntheses of mesoporous metal oxides by utilisation of supramolecular structure directors as well as the concept of structure replication will be discussed below.

Non-sol–gel approaches to the synthesis of mesoporous metal oxides for gas-sensing applications include chemical vapour deposition (CVD), spray pyrolysis, precipitation reactions and other methods. For example, Liu et al. used CVD to prepare SnO_2 thick films that consisted of agglomerated particles of about 30 nm diameter for ethanol sensing.[22] Korotcenkov et al. synthesised thin films of In_2O_3[23] and SnO_2[24] by spray pyrolysis; the products were built up from particles with sizes between 20 and 150 nm and were used for sensing of various gases, such as ozone, CO or H_2. Spray pyrolysis was also used by Mädler et al. who prepared thick films of SnO_2 for CO sensing by deposition of 10 nm sized particles; variation of the deposition time resulted in differences in film thickness of 9–40 μm.[25] Pinna and Niederberger et al. used a precipitation route from a non-aqueous system to prepare monodisperse, highly crystalline SnO_2 and In_2O_3 particles with sizes of 2–3 nm for NO_2, CO and CH_4 sensing;[26] the authors give a general survey over similar non-aqueous syntheses in ref. [27]. Leite et al. reported the synthesis of Nb_2O_5-doped SnO_2 nanoparticles by a polymeric precursor route, including some ethanol-gas-sensing measurements.[28]

Factors that Influence a Porous Gas Sensor's Performance

As mentioned above, the suitability of a semiconducting metal oxide material as a chemiresistor depends on several factors, many of which are correlated with each other. The most obvious factor is the chemical composition. Among the variety of appropriate materials, SnO_2 is by far the one most frequently used. In addition, WO_3, In_2O_3, Ga_2O_3 or ZnO have also been explored quite extensively; these and other metal oxide gas-sensing materials have recently been compiled in a rather exhaustive literature review.[8] In general, n-type semiconductors have turned out to be better suited than p-type. The sensitivity of the sensor can often be significantly enhanced by chemical modification of the metal oxide's surface. In particular, finely dispersed clusters of (noble) metals, such as Pt, Pd, Ag or Cu, may serve as catalysts for the chemical reaction between the analyte gas molecules and the semiconductor. Such foreign species increase the sensitivity and lower the temperature required for an optimum gas response by electronic and/or chemical interaction with the main sensing material.[29,30] The metal clusters can be created by impregnation of the sensor with a respective metal salt and subsequent chemical reduction or by deposition of pre-formed clusters from colloidal suspension; the resulting quantities of the metals typically lie in the region between 0.1 and 5 wt %. Instead of noble metals, foreign metal oxides have also been used as additives in semiconducting gas sensors in similar relative quantities.[31]

The next factor affecting the performance of a chemiresistor is its operation temperature. In general, the temperature-dependence of the sensitivity is marked by a maximum, typically at a few hundred degrees above room temperature, due to several reasons. On the one hand, the kinetics of both the reaction of the analyte gas with surface-adsorbed oxygen and the replacement of the latter from the gas phase must be taken into consideration. On the other hand, the kinetics of gas diffusion through the sensing layer plays another important role. Sakai and Yamazoe have suggested a model to explain the temperature dependency under the assumption that gas transport takes place entirely by Knudsen diffusion (see below), that is, without significant contribution of surface diffusion. The model successfully describes the frequently observed volcano-shaped temperature dependence of the sensitivity.[32,33]

The aspect of gas diffusion leads us to the rather complex realm of structural and textural parameters in the sensing layers. These are the grain size, the interconnectivity of the grains, the surface-to-volume ratio, the porosity and the film thickness. As pointed out above, the change in conductance of the sensing material occurs at the exterior regions of the grains. Beyond the depletion layer, the interior parts of the grains do not contribute to the gas response. As a consequence, the grain size affects the sensor performance quite substantially. In theory, grain sizes larger than twice the depletion layer thickness will be disadvantageous to the overall change in conductance of the material. Rothschild and Komem have carried out numerical simulations on SnO_2 grains with diameters between 5 and 80 nm which confirm this picture (Figure 4).[34] The model calculates the effective carrier concentration as a function of the surface state density. A steep increase is found when the surface state density reaches a critical value which corresponds to fully depleted grains; this critical value is proportional to the grain size. Thus, the sensitivity turns out to be proportional to the reciprocal grain size as long as the depletion region extends over the entire grain. The results from the theoretical calculations confirm experimental data obtained by Yamazoe et al. for the sensitivity of SnO_2 to H_2 or CO; the critical grain sizes were in the region of 5–15 nm.[31,35] For WO_3-based sensors for NO and NO_2 the respective values were determined between 25 and 35 nm.[36] The preparation of the sensing layer should therefore aim at reducing the grain size to approximately twice the depletion layer thickness. At this stage of the discussion it should be stressed that terms like "grain", "particle" or "crystallite" are often interchanged for one another. Here we use "grain" as a synonym of "single crystallite", regardless of whether or not (and to what extent) the crystallites may be agglomerated to form larger (polycrystalline) entities. This distinction will play a role later on. "Particle" will be used as a general term when the distinction between single grains and agglomerates is difficult and/or unnecessary.

Conventional sol–gel syntheses of mesoporous gas sensors yield particles with limited sizes in the nanometer region and (usually) approximately spherical shape, as discussed above. Theoretically, to maximise the specific surface area such spherical particles should be loosely packed, with infinitely small contact areas between each other (Figure 5a). On the other hand, calcination of the as-prepared material is required to obtain a sufficiently stable, porous network; such a process comprises sintering of the particles, increasing the degree of particle interconnectivity, but lowering the specific surface area (Figure 5b). For the gas-sensing performance a certain interconnectivity is necessary anyway, since the overall electronic conductance requires sufficient contact between neighbouring grains in order to facilitate percolation paths through the entire sensing layer.[37] Thus, a compromise between large specific surface area (realised by low grain interconnectivity) and stability/electronic conductance (high interconnectivity) is necessary. However, these parameters are still difficult to control; in particular, long-term op-

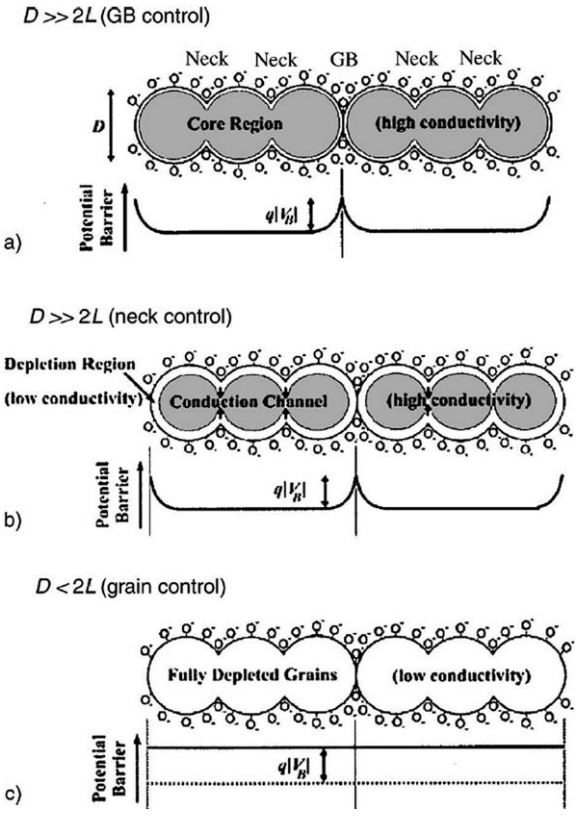

Figure 4. Model of the grain size effect in n-type semiconducting metal oxide gas sensors.[34] If the grains are large in comparison to the depletion layer thickness (a) the conductance (which is higher in the non-depleted core region) is controlled by grain boundaries. Necks between coalesced primary grains control the conductance when the grains become smaller (b), that is, when the depletion layer becomes thicker in relation to the grains size. If the grains are small enough to be fully depleted (c) the conductance is grain-controlled.

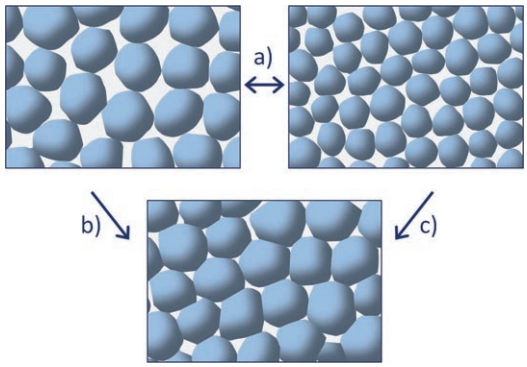

Figure 5. Schematic drawing of the mutual interplay between grain size, grain interconnectivity, pore size and specific surface area in a sol–gel-prepared porous material. a) In a loosely packed arrangement increasing the grain size (by choice of the synthesis conditions) leads to larger pores, but lower specific surface area. b) Sintering reduces both the pore size and the specific surface area while increasing the grain interconnectivity and, thus, the stability of the structure. c) Owing to ripening phenomena, sintering often goes along with growth of the grains.

eration of the sensor at elevated temperature will in many cases lead to subsequent sintering, changing the material's textural properties in the course of time. It should also be noted that calcination of the as-prepared material may substantially increase the particle size due to ripening phenomena (Figure 5c). This may be an undesired effect, but on the other hand can also be used as a tool to fine-tune the particle size. Shek et al. have systematically investigated how calcining sol–gel-prepared nanoparticulate SnO_2 (<5 nm) at various temperatures between 500 and 800 °C leads to different final particle sizes between approximately 10 and 30 nm; they also suggested a model to describe this effect.[38] Wu et al. have demonstrated that such ripening can be effectively inhibited by surface functionalisation of the as-prepared particles before calcination. They obtained crystalline particles of SnO_2, TiO_2 and ZrO_2 with fairly small sizes between 1.5 and 5 nm; after modification with a Pd salt the SnO_2 sample showed some interesting sensor activity to CO, although at comparably high concentration.[39] Leite et al. have shown that doping porous SnO_2 with Nb_2O_5 during the synthesis can effectively inhibit sintering- and ripening-induced grain growth (Figure 6).[28]

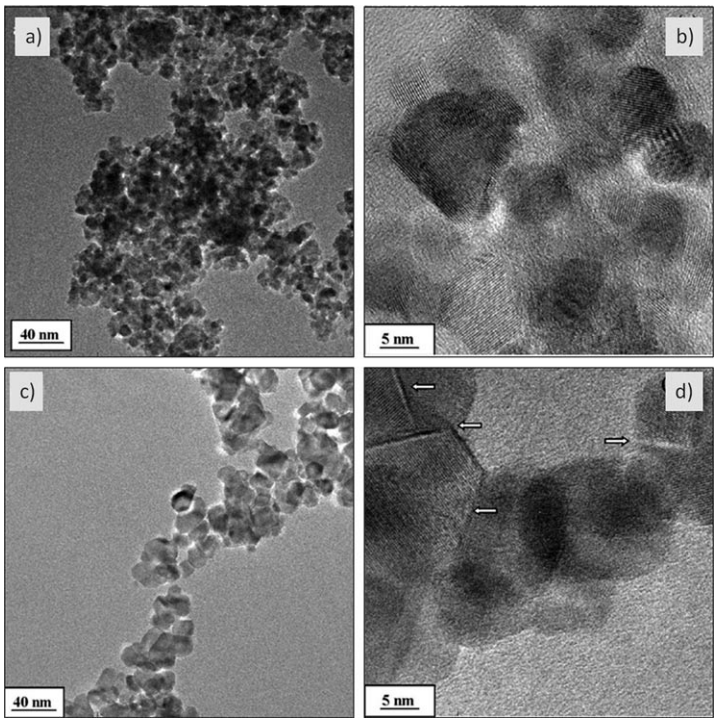

Figure 6. TEM images of Nb_2O_5-doped (a,b) and undoped SnO_2 nanoparticles (c,d). Doping inhibits sintering- and ripening-induced grain growth; the arrows indicate contact faces between coalesced grains.[28]

Another side-effect of sintering is the sometimes substantial change in porosity. The average pore size as well as the degree of interconnectivity of pores is affected by the particle size and the degree of particle interconnectivity. In theory, an increase in average particle size will result in larger pores, as depicted in Figure 5. It was found by Yamazoe et al. that increasing the grain size in SnO_2 thin films from 8.5 to 10 nm, while leaving the film thickness unchanged, resulted in higher sensitivity to H_2;[17a] similar results were obtained for H_2S.[17b] These observations seem to contradict the general trend that lower sensitivity is to be expected for larger grains, as discussed above. However, the authors argue that larger grain sizes mean larger mesopores and, thus, better diffusivity of the analyte gases, resulting in higher sensitivity. This demonstrates that pore size and grain size are correlated in sol–gel-synthesised sensor materials, with potentially opposite impact. Decreasing the grain size will on the one hand lead to higher sensitivity; on the other hand, the resultant smaller interparticle voids (mesopores) may very well be disadvantageous, an effect which may overcompensate the positive grain size effect. Furthermore, sintering during calcination of the sol–gel-prepared materials will cause a decrease in average pore size and, particularly, reduce the pore interconnectivity by creating narrower bottlenecks.[15] This last effect may again be disadvantageous to the diffusion of gas molecules, thus decreasing the overall sensor performance.

All these considerations show how in sol–gel-derived porous materials the average size and interconnectivity of both the grains and the pores, as well as the specific surface are highly interdependent and therefore quite difficult to control during chemical synthesis and post-synthetic treatment. Adjusting either of these parameters will very likely induce changes in other parameters which may or may not be desired. Thus, improved sensing properties are to be expected if the chemical synthesis of the porous materials offers the opportunity to treat both aspects (grain size, pore size) independently from each other. As we shall see, the synthesis of mesoporous materials by employing supramolecular structure directors as porogens or the utilisation of porous, rigid structure matrices offers such opportunities.

Diffusion-Controlled Selectivity and Self-Diagnosis

Let us now take a closer look at diffusion in mesopores. It is pretty evident that porosity plays a key role in the efficiency of semiconducting metal oxide gas sensors. On the one hand the pores should be wide enough for efficient diffusion of the gas molecules; the benefit of a high specific surface area must not be thwarted by limitations in the accessibility of the surface. On the other hand the surface-to-volume ratio directly depends on the pore size; the larger the pores are, the lower will be the specific surface area, provided the particle size (i.e., the "pore-wall thickness") is the same. Thus, a balance between these two complementary aspects needs to be chosen for the optimum sensor performance. In mesopores (pore radius $4<r<100$ nm) the mean free path of a gas molecule is determined by the pore walls rather than by adjacent molecules; in other words, a molecule is more likely to collide with the pore wall than with other gas molecules. Transport without external pressure is then described by Knudsen diffusion and the diffusion coefficient D_K is pro-

portional to the pore radius r, as shown in Equation (1) in which R is the universal gas constant and M is the molecular weight of the gas molecule.

$$D_K = 4r/3\sqrt{(2RT/\pi M)} \quad (1)$$

For larger pores, that is, macropores ($r > 25$ nm), gas transport occurs mainly by molecular diffusion (confinement by the pore boundaries is less significant), whereas in micropores ($r < 1$ nm) surface diffusion becomes predominant.[32,33] Surface diffusion will also have a more or less significant contribution in smaller mesopores; however, a basic model to successfully describe the temperature dependence of the sensitivity has been developed by assuming only Knudsen diffusion, as mentioned above.[32,33]

Equation (1) also shows that the Knudsen diffusivity of a gas in a mesoporous material depends significantly on the mass of the gas molecules. The heavier the molecules are, the slower will be their motion through the porous layer. This has significant consequences with respect to the gas selectivity of a porous sensor. Taking into account that the analyte gas molecules react with the pore walls, that is, they are consumed at a certain rate, a concentration gradient along the depth of the porous layer results. The mass-dependent differences in the diffusivity result in differences in these concentration profiles. Statistically, lighter molecules diffuse deeper into the sensing layer than heavier ones (Figure 7). If surface diffusion contributes to the overall

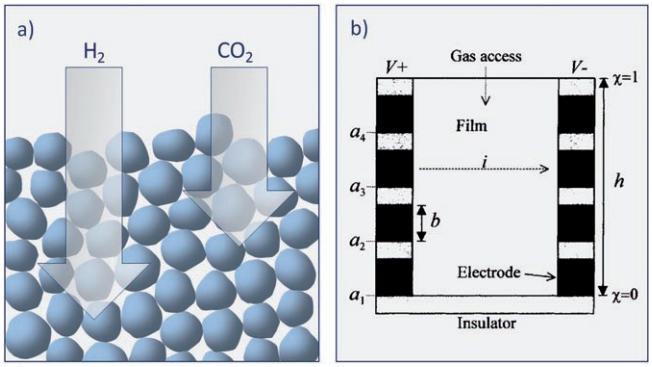

Figure 7. a) Schematic drawing showing how mass-dependent differences in the diffusivities of gases (e.g., H_2 and CO_2) lead to different concentration profiles within the porous sensing layer. Since the gases are consumed within the layer, their concentration decreases with increasing depth. b) Schematic drawing of a porous sensor film (of thickness h) with electrodes situated at various films depths a_i.[42b] Gases with different diffusivities will show distinct concentration profiles along the film depth. This setup affords gas-selective and self-diagnostic sensor devices.

mass transport (which is increasingly the case for smaller mesopores), then the differences in the diffusivity of different gases may be even more significant, since in addition to its molecular mass the interaction of the gas molecule with the pore wall surface will also be strongly gas-specific.

Egashira et al. showed that the interior regions of SnO_2 sensor thick films (ca. 200–300 μm thickness) are more sensitive towards H_2 than the film surfaces, while the opposite is true for the sensitivity to gases heavier than O_2 (methane, ethanol). The authors attributed this effect to differences in the diffusivities of the gases, but pointed out that different reaction kinetics must be taken into account as well.[40] Similar findings were reported by Sakai et al.[41] for SnO_2 thin films prepared according to the method described in reference [16]. The authors suggested a simple model on the basis of diffusivity and reactivity to calculate gas concentration profiles along idealised pores; the model assumes that gas transport occurs entirely by Knudsen diffusion. More specifically, Williams et al. showed how positioning different electrodes at different depths of thick film layers can be used as a tool for detecting various gases selectively within a single sensor device (Figure 7).[42] Moreover, such devices have the potential of being self-diagnostic, since poisoning, that is, inactivation of the sensor during long-term usage, will occur to a different degree at different depths of the sensing layers; a decrease in sensor response occurring at one electrode to a relatively higher degree than at the other electrodes is then a clear sign of such poisoning effects.[43] This is another example how porosity may be a powerful tool for improved sensor properties. If random design of the porosity (pore size distribution, pore geometry, pore interconnectivity) can be achieved during the chemical synthesis, both higher selectivity and reliability of the sensors will become possible.

However, all considerations regarding pore sizes and gas diffusivity of course need to take into account the aspect of film thickness and film quality, that is, presence or absence of cracks within the sensing layer. The above-mentioned ideas about utilising different gas diffusivities for varying the sensor's selectivity apply only for sufficiently thick sensing layers. Mass-dependent differences in the penetration depths will not be significant for thin films, that is, films with thicknesses in the sub-micrometer region. The preparation of thick films, on the other hand, bears the risk of introducing cracks during drying and calcination, which naturally will corrupt the thickness-dependent features. In the above-cited SnO_2 thin films prepared by spin-coating cracks occurred already for film thicknesses above 300 nm (Figure 8).[41] The generation of porous, crack-free thick films, for example, by slower drying or milder calcination conditions, is one of the key challenges in the synthesis of selective and potentially self-diagnostic gas sensors.

So far we have not taken into account that in sol–gel-derived porous materials the grains, that is, the single crystallites, of the sensing material, may be agglomerated to form larger entities. Such agglomeration is promoted by the calcination procedure. Voids between the constituting crystallites may still exist within the agglomerates, especially if calcination was carried out under comparably mild conditions, resulting in a low degree of sintering. Such intra-agglomerate (but inter-crystallite) voids are naturally narrower than those between the agglomerates (Figure 9). In other words, the porosity in the sensing layer may be bimodal: each agglomerate may contain small pores (micropores in the ex-

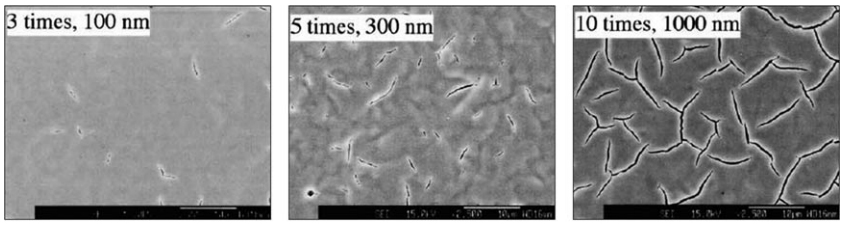

Figure 8. SEM images (top view, scale bars: 10 μm) of porous films prepared from sols containing 1.8% wt. SnO_2 by spin-coating; the number of spin-coating cycles and the resulting film thicknesses are indicated. A crack-free film is obtained only for 100 nm film thickness.[41]

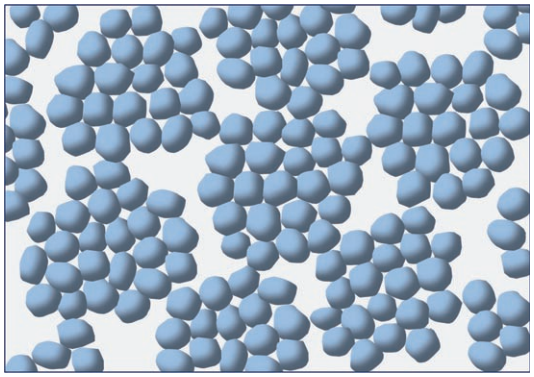

Figure 9. Schematic drawing of primary grains assembled into larger entities. The intra-agglomerate pores are smaller than the voids between adjacent agglomerates and, thus, rate-determining for the overall diffusivity of gas molecules.

treme case), while adjacent agglomerates are separated from each other by larger pores (mesopores). Gas diffusion is generally slower in smaller pores, as evident from Equation (1) for Knudsen diffusion. Apart from the pore size dependence of Knudsen diffusivity, the contribution of surface diffusion will become more and more significant in smaller mesopores; in micropores it will be dominant, since here the pore widths lie substantially below the mean free path of a gas molecule. Diffusion in the intra-agglomerate pores, if present, will therefore be rate-determining in the overall diffusivity. This situation was observed by Korotcenkov et al. who prepared SnO_2 thin films by ionic layer deposition and obtained crystallite sizes of approximately 6–7 nm; they found agglomerates with sizes as large as the film thickness (20–80 nm).[9,44] As we shall see below, modern synthesis methods, especially the utilisation of rigid structure matrices, make it possible to use high-temperature treatment to selectively diminish intra-agglomerate pores without affecting the ordered mesopore structure.

Synthesis of Ordered Mesoporous Metal Oxides by Utilisation of Amphiphilic Structure Directors

The utilisation of self-assembled supramolecular aggregates of amphiphilic species, such as surfactants or block co-polymers, as structure-directing units has become a standard technique for the synthesis of periodically ordered mesoporous materials.[45,46] During the sol–gel-based synthesis the amphiphilic molecules spontaneously self-organise to form micellar aggregates; these are incorporated into the growing solid network and are later removed (by calcination or solvent extraction) to yield regular arrays of channels or voids, the symmetry of which reflect the self-aggregation behaviour of the respective amphiphile (Figure 10). However, the self-assembly is usually substantially influenced by the presence

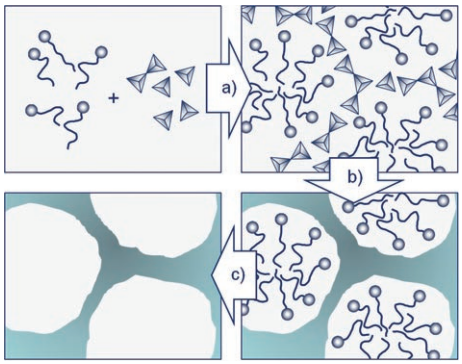

Figure 10. Schematic drawing of the synthesis of ordered, mesoporous materials by utilisation of amphiphilic species as structure directors. Starting from amphiphilic molecules and solute inorganic precursors, spontaneous self-assembly (a) leads to the formation of inorganic domains between periodically arranged micellar aggregates of amphiphiles until a solid network is formed (b); the amphiphilic molecules are finally removed, yielding periodic mesopores (c).

of the inorganic species forming the solid material; the mutual interaction between the various species leads to complex, co-operative mechanisms. This synthesis method is suitable mainly for materials that exhibit a tendency to form amorphous phases, especially SiO_2 and SiO_2-based materials,[47,48] or $AlPO_4$.[49] In many other cases the utilisation of such micellar structure directors has turned out not to be successful in generating periodically arranged, uniform mesopores. In particular, most metal oxides are not accessible as porous materials by this approach, one reason being the high lattice energies, which often lead to the formation of dense, non-porous phases.[50] However, two of the most important systems in gas sensing, SnO_2 and WO_3, happen to be accessible by amphiphilic structure direction. The respective products are obtained as powders, which can be conveniently applied to sensor substrates by drop-coating or spin-coating processes.

Stucky et al. prepared mesoporous SnO_2 and WO_3 with hexagonally arranged cylindrical pores of about 7 nm (SnO_2) and 5 nm (WO_3) diameter by using "P123" block copolymer as the amphiphilic structure-directing species. The polymer was removed by thermal decomposition at 450 °C,

after which the products exhibited specific surface areas of 180 $m^2 g^{-1}$ and 125 $m^2 g^{-1}$, respectively. The pore walls had a thickness of about 5 nm and, based on X-ray and electron diffraction data, consisted of small crystallites with mean sizes below 5 nm.[51] A surfactant with shorter chain length, cetyltrimethylammonium bromide (CTABr), was used by Wang and Ma et al. for the synthesis of SnO_2. The products had specific surface areas of 250–340 $m^2 g^{-1}$, narrow pore size distributions of 2–4 nm and were stable at temperatures below 350 °C. Gas-sensing tests revealed a high selectivity for H_2 against CO, methane or butane.[52] Egashira et al. prepared mesoporous SnO_2 by using the surfactant cetylpyridinium chloride; treatment of the products with phosphoric acid resulted in improved stability, leading to specific surface areas of 370 $m^2 g^{-1}$ after calcination at temperatures as high as 600 °C. Gas-sensing properties towards H_2 and NO_x were shown to be substantially increased by the large surface-to-volume ratio.[53] Tiemann and Kohl et al. have recently shown that mesoporous SnO_2 prepared by utilisation of CTABr surfactant exhibits high sensitivity to CO gas with very low cross sensitivity to water vapour as prepared to commercial SnO_2-based sensor devices (Figure 11).[54] Brinker et al. prepared SnO_2 with large specific surface areas of 500 $m^2 g^{-1}$ and spongelike mesopores of uniform size; thin films (230 nm) of the material, fabricated by spin-coating, showed high H_2 gas sensitivity at room temperature with low cross sensitivity to methane, CO and water.[55] Further syntheses of mesoporous SnO_2 by utilisation of amphiphilic structure directors were reported by several groups without investigation of the products' gas-sensing properties.[56–60]

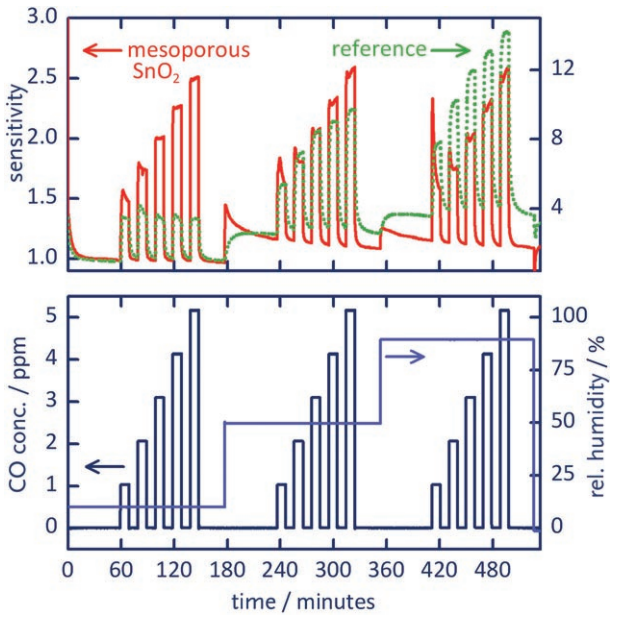

Figure 11. CO gas-sensing performance of a mesoporous SnO_2 sensor prepared by utilisation of CTAB as an amphiphilic structure director. The mesoporous samples shows lower cross sensitivity to water than a commercial SnO_2-based sensor.[54]

In addition to the above-described syntheses of mesoporous metal oxide powders, a modification of the amphiphilic structure-direction concept, the so-called EISA method (evaporation-induced self assembly), facilitates the preparation of thin films with well-ordered pores.[61,62] In this method the self-assembly of the amphiphiles and the resulting formation of the porous solid take place within a liquid film on the substrate from which the solvent is gradually removed by evaporation under controlled conditions. The resulting films exhibit high degrees of structural order and are often crack-free, which, as discussed above, may be highly advantageous for gas-sensing purposes. On the other hand the EISA concept only yields homogeneous films with limited thickness (sub-micrometer), which may not suffice for realising the idea of preparing porous sensors that are self-diagnostic and gas-selective based on characteristic film-depth-dependence concentration profiles (see above). Another problem is that EISA-prepared films often exhibit hexagonally arranged linear pores with the pore axes running parallel to the substrate plane, which means that the pores are not sufficiently accessible to the gas molecules; accessible pores, for example, with cubic symmetries, are less frequently obtained. Nevertheless, over the last few years a variety of mesoporous metal oxide thin films prepared by the EISA method have been reported, many of which may be of interest in gas sensing. Grosso and Sanchez et al. used block co-polymers to synthesise mesoporous TiO_2 films of 50–700 nm thickness; the pores had sizes between 2.5 and 8 nm and were arranged in cubic symmetry.[63] The same authors also prepared films of ZrO_2–Y_2O_3 and ZrO_2–CeO_2 mixed oxides.[64] Another synthesis of mesoporous TiO_2 films was reported by Ozin et al.[65] Smarsly et al. used a special block co-polymer ("KLE") to prepare several mesoporous metal oxide films with interesting pore structures, including TiO_2,[66a] CeO_2,[66b] WO_3[66c] and, most recently, SnO_2.[66d] These films had usually thicknesses around 100 nm and consisted of grains between 2 nm (SnO_2) and 14 nm (WO_3) in size (Figure 12). Further reports on mesoporous SnO_2 films were made by Hillhouse and Urade[67] and by Lee et al.[68]

Synthesis of Ordered Mesoporous Metal Oxides by Structure Replication (Nanocasting)

Recently it was shown that ordered, mesoporous metal oxides can be synthesised by structure replication (nanocasting), utilising mesoporous silica as a rigid matrix.[69–72] This method has opened up new opportunities to obtain mesoporous materials that were formerly not available. Structure replication comprises two consecutive synthesis steps: the mesoporous silica is first prepared by utilisation of amphiphilic structure directors, as described above. The silica pores are then filled with a molecular precursor, for example, a metal salt, which is converted in situ into the desired

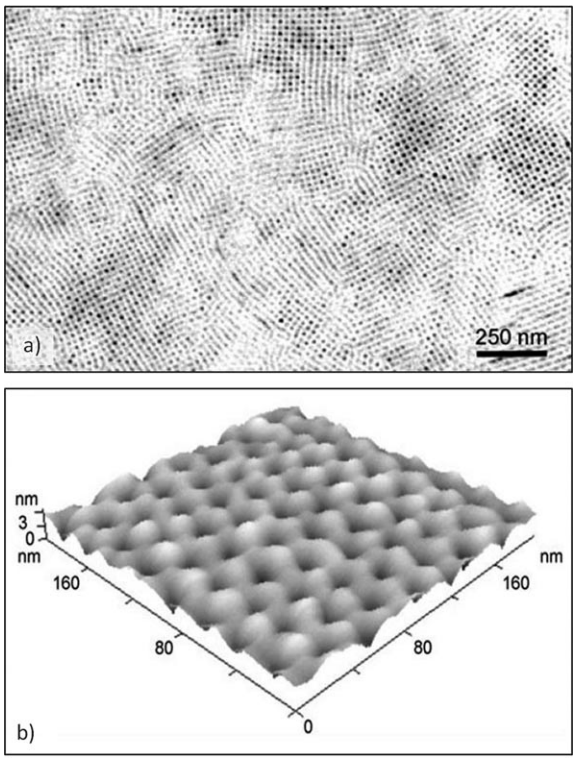

Figure 12. a) SEM and b) AFM image of a mesoporous WO_3 film prepared by the EISA method, showing large crack-free domains and uniform, accessible pores.[66c]

metal oxide. Finally the silica matrix is removed by treatment with hydrofluoric acid (HF) or concentrated sodium hydroxide solution (NaOH). Thus, the metal oxide is obtained as the negative replica of the silica matrix (Figure 13). This has led to a large number of new, mesoporous metal oxides, many of which are of interest in the field of gas sensing. For example, Zhao et al. have prepared mesoporous In_2O_3 by utilising silica matrices with various symmetries in the pore systems; selected area electron diffraction (SAED) indicates large crystalline domains, extending over several repeat distances of the periodic pore arrangement.[73] In the same fashion several other mesoporous materials with similar structural properties were reported, including WO_3,[74] Fe_2O_3,[75] Cr_2O_3,[76] CeO_2,[74c,77,78] Co_3O_4,[73,76b,79–84] Mn_xO_y[81b,85] and SnO_2.[81b] For some metal oxides mesoporous silica is not suitable as a matrix for structure replication, because the silica removal needs to be carried out under chemically harsh conditions. Amphoteric oxides, such as ZnO, are not stable against treatment with either HF or NaOH aqueous solution. In such cases, mesoporous carbon offers an alternative as a structure matrix, since its removal can be accomplished by controlled thermal decomposition. Mesoporous carbon is itself prepared by structure replication from silica;[86] thus, the entire process can be envisaged as a double replication procedure, that is, silica-to-carbon, followed by carbon-to-metal oxide. This concept has afforded several more new mesoporous materials with well-defined pore systems, such as TiO_2,[87] ZrO2,[87] Al_2O_3,[87,88] ZnO,[89,90] CeO_2,[91] CuO[92] and MgO.[93] Some mesoporous metal oxides prepared by structure replication have been shown to exhibit promising gas-sensing performance: mesoporous Co_3O_4, synthesised by using mesoporous SBA-15 silica as the structure matrix (Figure 14), turned out to be more sensitive to CO at lower operation temperature than a non-porous Co_3O_4 sample.[84] Similar findings were obtained for mesoporous ZnO synthesised by utilisation of mesoporous CMK-3 carbon as the structure matrix.[89b]

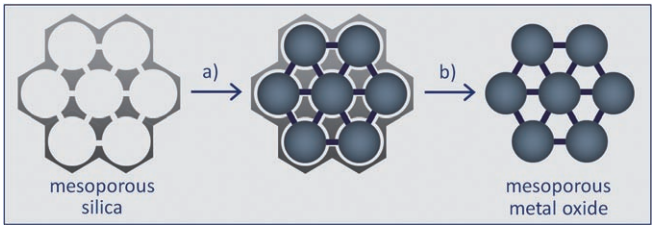

Figure 13. Schematic diagram showing the synthesis of mesoporous metal oxides by using porous silica as a structure matrix. The metal oxide is formed inside the pores of the silica matrix (a) which is then removed (b), yielding the metal oxide as its negative replica.

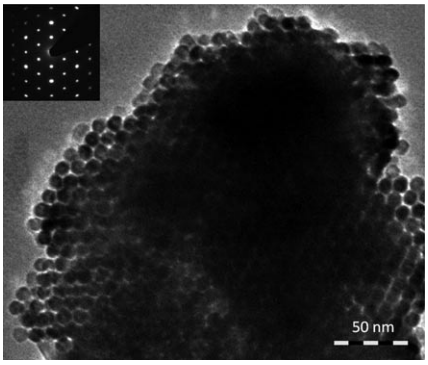

Figure 14. TEM image and selected area electron diffraction (SAED) pattern of mesoporous Co_3O_4 prepared by structure replication (nanocasting).[84]

Apart from being applicable in a more universal fashion, the structure replication method bears another important advantage over the utilisation of amphiphiles as structure directors, as well as over regular sol–gel syntheses without structure directors. The latter concepts are tied to close limitations with respect to the synthesis temperature, since they involve liquid (usually aqueous) synthesis media. The synthesis needs to be carried out at temperatures below about 200 °C, requiring pressure-tight autoclave vessels for hydrothermal conditions. However, to obtain stable and crystalline metal oxides, higher temperatures are usually necessary; they can only be established post-synthetically, for example, during the removal of the amphiphilic species, which may be harmful to the mesoscopic structure. In many cases the porosity and specific surface area are diminished or completely

lost during post-synthetic thermal treatment. In contrast, rigid matrices, either silica or carbon, can withstand high temperatures during the formation of the desired metal oxides inside their pore systems. Serving as a rigid skeleton, a solid-state template allows for temperatures of several hundred degrees without loss in periodic structure. Thus, higher degrees of crystallinity and larger single-crystalline domains are possible.

The concept of using structure directors or rigid structure matrices for the synthesis of mesoporous metal oxide gas sensors offers a number of substantial advantages over conventional synthesis methods. As discussed above, sol–gel syntheses (without structure direction) do not allow to randomly manipulate pore size/pore interconnectivity, grain size/grain interconnectivity, specific surface area and other structural factors independently. Structure replication is a versatile means to create well-defined mesopores with narrow pore-size distribution and high specific surface areas. Rigid structure matrices make it possible to prevent undesired changes in the pore structure upon high-temperature treatment (Figure 15). Such treatment plays a vital role in improving the material's grain interconnectivity and long-term thermal stability; intra-agglomerate porosity can be prevented without damage to the inter-agglomerate mesopores (compare Figure 9). Thus, the concept of structure replication offers new opportunities to decouple some key structural parameters from each other, facilitating individual control over each on of them.

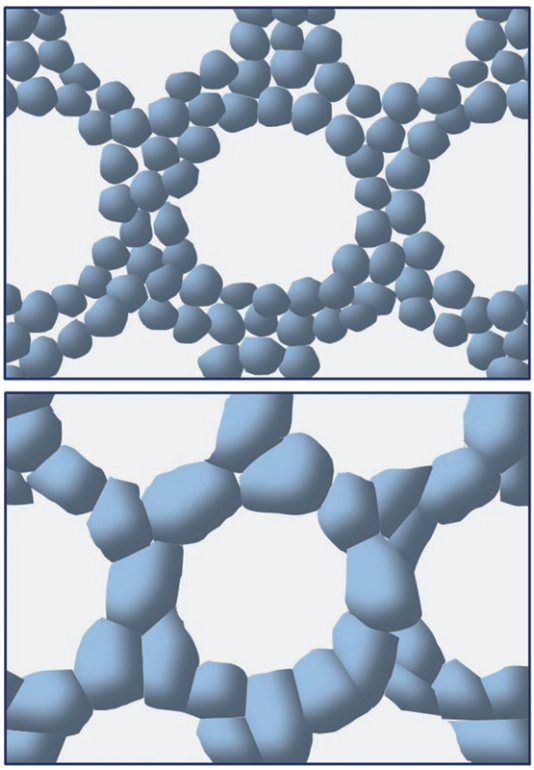

Figure 15. Schematic drawing showing how grain size effects due to sintering and/or ripening does not affect stability and size of the mesopores in materials prepared by structure replication. High-temperature treatment of the metal oxide is possible before removal of the structure matrix, which serves as a rigid skeleton, preventing structural damage.

Conclusion

Mesoporosity plays a vital role in the application of semiconducting metal oxides as gas sensors. Apart from exhibiting high sensitivities due to large specific surface areas, sensors with well-defined porosity offer powerful opportunities with respect to selectivity, self-diagnosis, low operation temperatures or long-term stability. Conventional synthesis methods do not allow efficient and individual control over many key structural parameters, such as grain size, grain interconnectivity, pore size and pore architecture. New synthesis concepts of structure direction and structure replication (nanocasting) provide new opportunities to create materials with defined mesoporosity and improved gas-sensing properties.

Acknowledgements

The author thanks Prof. Dr. C.-D. Kohl for ongoing and fruitful discussion and for critical revision of this manuscript, as well as Prof. Dr. M. Fröba for continuous support.

[1] T. Seiyama, A. Kato, K. Fujiishi, M. Nagatani, *Anal. Chem.* **1962**, *34*, 1502–1503.
[2] J. R. Stetter, W. R. Penrose, S. Yao, *J. Electrochem. Soc.* **2003**, *150*, S11-S16.
[3] N. Yamazoe, *Sens. Actuators B* **2005**, *108*, 2–14.
[4] D. Kohl, *J. Phys. D* **2001**, *34*, R125–R149.
[5] N. Barsan, M. Schweizer-Berberich, W. Göpel, *Fresenius J. Anal. Chem.* **1999**, *365*, 287–304.
[6] N. Barsan, U. Weimar, *J. Phys. Condens. Matter* **2003**, *15*, R813-R839.
[7] N. Yamazoe, G. Sakai, K. Shimanoe, *Catal. Surv. Asia* **2003**, *7*, 63–75.
[8] G. Eranna, B. C. Joshi, D. P. Runthala, R. P. Gupta, *Crit. Rev. Solid State Mater. Sci.* **2004**, *29*, 111–188.
[9] G. Korotcenkov, *Sens. Actuators B* **2005**, *107*, 209–232.
[10] M. E. Franke, T. J. Koplin, U. Simon, *Small* **2006**, *2*, 36–50.
[11] A. Gurlo, R. Riedel, *Angew. Chem.* **2007**, *119*, 3900–3923; *Angew. Chem. Int. Ed.* **2007**, *46*, 3826–3848.
[12] A. Gurlo, *ChemPhysChem* **2006**, *7*, 2041–2052.
[13] N. Barsan, U. Weimar, *J. Electroceram.* **2001**, *7*, 143–167.
[14] K. S. W. Sing, D. H. Everett, R. A. W. Haul, L. Moscou, R. A. Pierotti, J. Rouquérol, T. Siemieniewska, *Pure Appl. Chem.* **1985**, *57*, 603–619.
[15] C. J. Brinker, G. W. Scherer, *Sol–gel Science: The Physics and Chemistry of Sol–gel Processing*, Academic Press, San Diego, **1990**.
[16] a) N. S. Baik, G. Sakai, N. Miura, N. Yamazoe, *J. Am. Ceram. Soc.* **2000**, *83*, 2983–2987; b) N. S. Baik, G. Sakai, N. Miura, N. Yamazoe, *Sens. Actuators B* **2000**, *63*, 74–79; c) N. S. Baik, G. Sakai, K. Shimanoe, N. Miura, N. Yamazoe, *Sens. Actuators B* **2000**, *65*, 97–100.
[17] a) D. D. Vuong, G. Sakai, K. Shimanoe, N. Yamazoe, *Sens. Actuators B* **2004**, *103*, 386–391; b) D. D. Vuong, G. Sakai, K. Shimanoe, N. Yamazoe, *Sens. Actuators B* **2005**, *105*, 437–442.
[18] F. Lu, S. Chen, S. Peng, *Catal. Today* **1996**, *30*, 183–188.
[19] F. Lu, Y. Liu, M. Dong, X. Wang, *Sens. Actuators B* **2000**, *66*, 225–227.

[20] A. Jitianu, Y. Altindag, M. Zaharescu, M. Wark, *J. Sol–gel Sci. Technol.* **2003**, *26*, 483–488.
[21] G. S. Devi, T. Hyodo, Y. Shimizu, M. Egashira, *Sens. Actuators B* **2002**, *87*, 122–129.
[22] Y. Liu, E. Koep, M. Liu, *Chem. Mater.* **2005**, *17*, 3997–4000.
[23] a) G. Korotcenkov, V. Brinzari, A. Cerneavschi, M. Ivanov, A. Cornet, J. Morante, A. Cabot, J. Arbiol, *Sens. Actuators B* **2004**, *98*, 122–129; b) G. Korotcenkov, A. Cerneavschi, V. Brinzari, A. Vasiliev, M. Ivanov, A. Cornet, J. Morante, A. Cabot, J. Arbiol, *Sens. Actuators B* **2004**, *99*, 297–303.
[24] G. Korotcenkov, V. Brinzari, J. Schwank, M. DiBattista, A. Vasiliev, *Sens. Actuators B* **2001**, *77*, 244–252.
[25] L. Mädler, A. Roessler, S. E. Pratsinis, T. Sahm, A. Gurlo, N. Barsan, U. Weimar, *Sens. Actuators B* **2006**, *114*, 283–295.
[26] N. Pinna, G. Neri, M. Antonietti, M. Niederberger, *Angew. Chem.* **2004**, *116*, 4445–4449; *Angew. Chem. Int. Ed.* **2004**, *43*, 4345–4349.
[27] a) M. Niederberger, G. Garnweitner, *Chem. Eur. J.* **2006**, *12*, 7283–7302; b) M. Niederberger, G. Garnweitner, N. Pinna, G. Neri, *Prog. Solid State Chem.* **2006**, *33*, 59–70.
[28] E. R. Leite, I. T. Weber, E. Longo, J. A. Varela, *Adv. Mater.* **2000**, *12*, 956–968.
[29] S. Matsushima, Y. Teraoka, N. Miura, N. Yamazoe, *Jpn. J. Appl. Phys. Part 1* **1988**, *27*, 1798–1802.
[30] G. Korotcenkov, V. Brinzari, Y. Boris, M. Ivanov, J. Schwank, J. Morante, *Thin Solid Films* **2003**, *436*, 119–126.
[31] C. Xu, J. Tamaki, N. Miura, N. Yamazoe, *Sens. Actuators B* **1991**, *3*, 147–155.
[32] G. Sakai, N. Matsunaga, K. Shimanoe, N. Yamazoe, *Sens. Actuators B* **2001**, *80*, 125–131.
[33] N. Matsunaga, G. Sakai, K. Shimanoe, N. Yamazoe, *Sens. Actuators B* **2003**, *96*, 226–233.
[34] A. Rothschild, Y. Komem, *J. Appl. Phys.* **2004**, *95*, 6374–6380.
[35] N. Yamazoe, *Sens. Actuators B* **1991**, *5*, 7–19.
[36] J. Tamaki, Z. Zhang, K. Fujimori, M. Akiyama, T. Harada, N. Miura, N. Yamazoe, *J. Electrochem. Soc.* **1994**, *141*, 2207–2210.
[37] M. Ulrich, A. Bunde, C. D. Kohl, *Appl. Phys. Lett.* **2004**, *85*, 242–244.
[38] C. H. Shek, J. K. L. Lai, G. M. Lin, *Nanostruct. Mater.* **1999**, *11*, 887–893.
[39] N. L. Wu, S. Y. Wang, I. A. Rusakova, *Science* **1999**, *285*, 1375–1377.
[40] a) Y. Shimizu, Y. Nakamura, M. Egashira, *Sens. Actuators B* **1993**, *13*, 128–131; b) Y. Shimizu, T. Maekawa, Y. Nakamura, M. Egashira, *Sens. Actuators B* **1998**, *46*, 163–168.
[41] G. Sakai, N. S. Baik, N. Miura, N. Yamazoe, *Sens. Actuators B* **2001**, *77*, 116–121.
[42] a) D. E. Williams, G. S. Henshaw, K. F. E. Pratt, R. Peat, *J. Chem. Soc. Faraday Trans.* **1995**, *91*, 4299–4307; b) D. E. Williams, K. F. E. Pratt, *J. Chem. Soc. Faraday Trans.* **1995**, *91*, 1961–1966.
[43] P. McGeehin, P. T. Moseley, D. E. Williams, *Sens. Rev.* **1994**, *14*, 13–19.
[44] G. Korotcenkov, V. Macsanov, V. Tolstoy, V. Brinzari, J. Schwank, G. Faglia, *Sens. Actuators B* **2003**, *96*, 602–609.
[45] J. S. Beck, J. C. Vartuli, W. J. Roth, M. E. Leonowicz, C. T. Kresge, K. D. Schmitt, C. T. W. Chu, D. H. Olson, E. W. Sheppard, S. B. McCullen, J. B. Higgins, J. L. Schlenker, *J. Am. Chem. Soc.* **1992**, *114*, 10834–10843.
[46] D. Zhao, Q. Huo, J. Feng, B. F. Chmelka, G. D. Stucky, *J. Am. Chem. Soc.* **1998**, *120*, 6024–6036.
[47] G. J. A. A. Soler-Illia, C. Sanchez, B. Lebeau, J. Patarin, *Chem. Rev.* **2002**, *102*, 4093–4138.
[48] Y. Wan, Y. Shi, D. Zhao, *Chem. Commun.* **2007**, 897–926.
[49] M. Tiemann and M. Fröba, *Chem. Mater.* **2001**, *13*, 3211–3217.
[50] F. Schüth, *Chem. Mater.* **2001**, *13*, 3184–3195.
[51] a) P. Yang, D. Zhao, D. I. Margolese, B. F. Chmelka, G. D. Stucky, *Nature* **1998**, *396*, 152–155; b) P. Yang, D. Zhao, D. I. Margolese, B. F. Chmelka, G. D. Stucky, *Chem. Mater.* **1999**, *11*, 2813–2826.
[52] a) Y. Wang, C. Ma, X. Sun, H. Li, *Microporous Mesoporous Mater.* **2001**, *49*, 171–178; b) Y. D. Wang, C. L. Ma, X. H. Wu, X. D. Sun, H. D. Li, *Sens. Actuators B* **2002**, *85*, 270–276; c) Y. Wang, C. Ma, X. Sun, H. Li, *J. Colloid Interface Sci.* **2005**, *286*, 627–631.
[53] a) T. Hyodo, N. Nishida, Y. Shimizu, Y. Egishara, *Sens. Actuators B* **2002**, *83*, 209–215; b) T. Hyodo, S. Abe, Y. Shimizu, M. Egashira, *Sens. Actuators B* **2003**, *93*, 590–600.
[54] T. Wagner, C.-D. Kohl, M. Fröba, M. Tiemann, *Sensors* **2006**, *6*, 318–323.
[55] G. De, R. Köhn, G. Xomeritakis, C. J. Brinker, *Chem. Commun.* **2007**, 1840–1842.
[56] K. G. Severin, T. M. Abdel-Fattah, T. J. Pinnavaia, *Chem. Commun.* **1998**, 1471–1472.
[57] G. J. Li, S. Kawi, *Talanta* **1998**, *45*, 759–766.
[58] F. Chen, M. Liu, *Chem. Commun.* **1999**, 1829–1830.
[59] T. Wang, Z. Ma, F. Xu, Z. Jiang, *Electrochem. Commun.* **2003**, *5*, 599–602.
[60] N. L. Wu, C. Y. Tung, *J. Am. Ceram. Soc.* **2004**, *87*, 1741–1746.
[61] Y. Lu, R. Ganguli, C. A. Drewien, M. T. Anderson, C. J. Brinker, W. Gong, Y. Guo, H. Soyez, B. Dunn, M. H. Huang, J. I. Zink, *Nature* **1997**, *389*, 364–368.
[62] C. J. Brinker, Y. Lu, A. Sellinger, H. Fan, *Adv. Mater.* **1999**, *11*, 579–585.
[63] a) E. L. Crepaldi, G. J. D. A. Soler-Illia, D. Grosso, M. Sanchez, *New J. Chem.* **2003**, *27*, 9–13; b) D. Grosso, G. J. D. A. Soler-Illia, E. L. Crepaldi, F. Cagnol, C. Sinturel, A. Bourgeois, A. Brunet-Bruneau, H. Amenitsch, P. A. Albouy, C. Sanchez, *Chem. Mater.* **2003**, *15*, 4562–4570; c) E. L. Crepaldi, G. J. D. A. Soler-Illia, D. Grosso, F. Cagnol, F. Ribot, C. Sanchez, *J. Am. Chem. Soc.* **2003**, *125*, 9770–9786.
[64] E. L. Crepaldi, G. J. D. A. Soler-Illia, A. Bouchara, D. Grosso, D. Durand, C. Sanchez, *Angew. Chem.* **2003**, *115*, 361–365; *Angew. Chem. Int. Ed.* **2003**, *42*, 347–351.
[65] S. Y. Choi, M. Mamak, N. Coombs, N. Chopra, G. A. Ozin, *Adv. Funct. Mater.* **2004**, *14*, 335–344.
[66] a) B. Smarsly, D. Grosso, T. Brezesinski, N. Pinna, C. Boissière, M. Antonietti, C. Sanchez, *Chem. Mater.* **2004**, *16*, 2948–2952; b) T. Brezesinski, C. Erpen, K. I. Iimura, B. Smarsly, *Chem. Mater.* **2005**, *17*, 1683–1690; c) T. Brezesinski, D. Fattakhova-Rohfing, S. Sallard, M. Antonietti, B. M. Smarsly, *Small* **2006**, *2*, 1203–1211; d) T. Brezesinski, A. Fischer, K. I. Iimura, C. Sanchez, D. Grosso, M. Antonietti, B. M. Smarsly, *Adv. Funct. Mater.* **2006**, *16*, 1433–1440.
[67] V. N. Urade, H. W. Hillhouse, *J. Phys. Chem. B* **2005**, *109*, 10538–10541.
[68] a) J. H. Pan, W. I. Lee, *Chem. Mater.* **2006**, *18*, 847–853; b) J. H. Pan, S. Y. Chai, C. Lee, S. E. Park, W. I. Lee, *J. Phys. Chem. C* **2007**, *111*, 5582–5587.
[69] F. Schüth, *Angew. Chem.* **2003**, *115*, 3730–3750; *Angew. Chem. Int. Ed.* **2003**, *42*, 3604–3622.
[70] H. Yang, D. Zhao, *J. Mater. Chem.* **2005**, *15*, 1217–1231.
[71] A. H. Lu, F. Schüth, *Adv. Mater.* **2006**, *18*, 1793–1805.
[72] Y. Wan, H. Yang, D. Zhao, *Acc. Chem. Res.* **2006**, *39*, 423–432.
[73] a) B. Tian, X. Liu, H. Yang, S. Xie, C. Yu, B. Tu, D. Zhao, *Adv. Mater.* **2003**, *15*, 1370–1374; b) H. Yang, Q. Shi, B. Tian, Q. Lu, F. Gao, S. Xie, J. Fan, C. Yu, B. Tu, D. Zhao, *J. Am. Chem. Soc.* **2003**, *125*, 4724–4725; c) B. Tian, X. Liu, L. A. Solovyov, Z. Liu, H. Yang, Z. Zhang, S. Xie, F. Zhang, B. Tu, C. Yu, O. Terasaki, D. Zhao, *J. Am. Chem. Soc.* **2004**, *126*, 865–875.
[74] a) K. Zhu, H. He, S. Xie, X. Zhang, W. Zhou, S. Jin, B. Yue, *Chem. Phys. Lett.* **2003**, *377*, 317–321; b) B. Yue, H. L. Tang, Z. P. Kong, K. Zhu, C. Dickinson, W. Z. Zhou, H. Y. He, *Chem. Phys. Lett.* **2005**, *407*, 83–86; c) E. Rossinyol, J. Arbiol, F. Peiro, A. Cornet, J. R. Morante, B. Tian, D. Zhao, *Sens. Actuators B* **2005**, *109*, 57–63.
[75] F. Jiao, A. Harrison, J. C. Jumas, A. V. Chadwick, W. Kockelmann, P. G. Bruce, *J. Am. Chem. Soc.* **2006**, *128*, 5468–5474.
[76] a) K. Jiao, B. Zhang, B. Yue, Y. Ren, S. Liu, S. Yan, C. Dickinson, W. Zhou, H. He, *Chem. Commun.* **2005**, 5618–5619; b) C. Dickinson, W. Zhou, R. P. Hodgkins, Y. Shi, D. Zhao, H. He, *Chem. Mater.* **2006**, *18*, 3088–3095.
[77] S. C. Laha, R. Ryoo, *Chem. Commun.* **2003**, 2138–2139.

[78] W. Shen, X. Dong, Y. Zhu, H. Chen, J. Shi, *Microporous Mesoporous Mater.* **2005**, *85*, 157–162.
[79] Y. Wang, C. M. Yang, W. Schmidt, B. Spliethoff, E. Bill, F. Schüth, *Adv. Mater.* **2005**, *17*, 53–56.
[80] F. Jiao, K. M. Shaju, P. G. Bruce, *Angew. Chem.* **2005**, *117*, 6708–6711; *Angew. Chem. Int. Ed.* **2005**, *44*, 6550–6553.
[81] a) J.-H. Smått, B. Spliethoff, J. B. Rosenholm, M. Lindén, *Chem. Commun.* **2004**, 2188–2189; b) J.-H. Smått, C. Weidenthaler, J. B. Rosenholm, M. Lindén, *Chem. Mater.* **2006**, *18*, 1443–1450.
[82] Y. M. Wang, Z. Y. Wu, H. J. Wang, J. H. Zhu, *Adv. Funct. Mater.* **2006**, *16*, 2374–2386.
[83] a) Y. Wang, C.-M. Yang, W. Schmidt, B. Spliethoff, E. Bill, F. Schüth, *Adv. Mater.* **2005**, *17*, 53–56; b) A. Rumplecker, F. Kleitz, E. L. Salabas, F. Schüth, *Chem. Mater.* **2007**, *19*, 485–496.
[84] T. Wagner, J. Roggenbuck, C.-D. Kohl, M. Fröba, M. Tiemann, *Stud. Surf. Sci. Catal.* **2007**, *165*, 347–350.
[85] M. Imperor-Clerc, D. Bazin, M. D. Appay, P. Beaunier, A. Davidson, *Chem. Mater.* **2004**, *16*, 1813–1821.
[86] a) R. Ryoo, S. H. Joo, S. Jun, *J. Phys. Chem. B* **1999**, *103*, 7743–7746; b) S. Jun, S. H. Joo, R. Ryoo, M. Kruk, M. Jaroniec, Z. Liu, T. Ohsuna, O. Terasaki, *J. Am. Chem. Soc.* **2000**, *122*, 10712–10713.
[87] A. Dong, N. Ren, Y. Tang, Y. Wang, Y. Zhang, W. Hua, Z. Gao, *J. Am. Chem. Soc.* **2003**, *125*, 4976–4978.
[88] Q. Liu, A. Wang, X. Wang, T. Zhang, *Chem. Mater.* **2006**, *18*, 5153–5155.
[89] a) T. Waitz, M. Tiemann, P. J. Klar, J. Sann, J. Stehr, B. K. Meyer, *Appl. Phys. Lett.* **2007**, *90*, 123108; b) T. Wagner, T. Waitz, J. Roggenbuck, M. Fröba, C.-D. Kohl, M. Tiemann, *Thin Solid Films* **2007**, in press.
[90] S. Polarz, A. V. Orlov, F. Schüth, A.-H. Lu, *Chem. Eur. J.* **2007**, *13*, 592–597.
[91] J. Roggenbuck, H. Schäfer, T. Tsoncheva, C. Minchev, J. Hanss, M. Tiemann, *Microporous Mesoporous Mater.* **2007**, *101*, 335–341.
[92] X. Lai, X. Li, W. Geng, J. Tu, J. Li, S. Qiu, *Angew. Chem.* **2007**, *119*, 752–755; *Angew. Chem. Int. Ed.* **2007**, *46*, 738–741.
[93] a) J. Roggenbuck, M. Tiemann, *J. Am. Chem. Soc.* **2005**, *127*, 1096–1097; b) J. Roggenbuck, G. Koch, M. Tiemann, *Chem. Mater.* **2006**, *18*, 4151–4156.

Published online: August 23, 2007

